Physically-based landslide prediction over a large region

Scaling low-resolution hydrological model results for high-resolution slope stability assessment

Wang, Sheng; Zhang, Ke; van Beek, Ludovicus P.H.; Tian, Xin; Bogaard, Thom A.

DOI
10.1016/j.envsoft.2019.104607

Publication date
2020

Document Version
Final published version

Published in
Environmental Modelling and Software

Citation (APA)
Wang, S., Zhang, K., van Beek, L. P. H., Tian, X., & Bogaard, T. A. (2020). Physically-based landslide prediction over a large region: Scaling low-resolution hydrological model results for high-resolution slope stability assessment. *Environmental Modelling and Software*, *124*, Article 104607. https://doi.org/10.1016/j.envsoft.2019.104607

Environmental Modelling and Software 124 (2020) 104607

Contents lists available at ScienceDirect

Environmental Modelling and Software

journal homepage: http://www.elsevier.com/locate/envsoft

Physically-based landslide prediction over a large region: Scaling low-resolution hydrological model results for high-resolution slope stability assessment

Sheng Wang [a,b], Ke Zhang [a,*], Ludovicus P.H. van Beek [c], Xin Tian [b], Thom A. Bogaard [b]

[a] State Key Laboratory of Hydrology-Water Resources and Hydraulic Engineering, College of Hydrology and Water Resources, and CMA-HHU Joint Laboratory for HydroMeteorological Studies, Hohai University, Nanjing, Jiangsu, 210098, China
[b] Department of Water Management, Delft University of Technology, 2600, GA, Delft, the Netherlands
[c] Department of Physical Geography, Utrecht University, 3508TC, Utrecht, the Netherlands

ARTICLE INFO

Keywords:
Landslide prediction
Hydrological model
Infinite slope model
Scaling

ABSTRACT

Rainfall-triggered shallow landslides are widespread natural hazards around the world, causing many damages to human lives and property. In this study, we focused on predicting landslides in a large region by coupling a 1 km-resolution hydrological model and a 90 m-resolution slope stability model, where a downscaling method for soil moisture via topographic wetness index was applied. The modeled hydrological processes show generally good agreements with the observed discharges: relative biases and correlation coefficients at three validation stations are all <20% and >0.60, respectively. The derived scaling law for soil moisture allows for near-conservative downscaling of the original 1-km soil moisture to 90-m resolution for slope stability assessment. For landslide prediction, the global accuracy and true positive rate are 97.2% and 66.9%, respectively. This study provides an effective and computationally efficient coupling method to predict landslides over large regions in which fine-scale topographical information is incorporated.

1. Introduction

Rainfall-triggered shallow landslides are worldwide natural hazard (Hong et al., 2006; An et al., 2016), causing a large number of fatalities and property losses (Liao et al., 2010; He et al., 2016; Godt et al., 2009). Globally, landslide hazards cause approximately 1000 deaths and USD 4 billion losses per year (Pradhan and Youssef, 2010). China is severely affected by landslide hazards, which has led to 1100 fatalities and 5–10 billion US dollars since 2000 (Hong et al., 2017). Due to frequent fatalities and extensive property damages that landslide hazard may cause (Papathoma-Kohle et al., 2015), it is essential to investigate and predict landslide hazards to avoid the damages (Zhang et al., 2019). Methods for hazard assessment range from heuristic susceptibility approaches (Fookes, 1997; Guzzetti et al., 2000; Griffiths and Edwards, 2001; Griffiths, 2002) to lumped regional empirical rainfall thresholds (Bogaard and Greco, 2018; Glade et al., 2000; Caine, 1980; Guzzetti et al., 2007, 2008) to detailed physical-based coupled hydrological-slope stability models (He et al., 2016; Zhang et al., 2016; Wilkinson et al., 2002; Alvioli and Baum, 2016; Montrasio and Valentino, 2016a, b; Van Asch et al., 2007). However, most of the studies focused on a single slope or landslide event in a relatively small catchment, usually in the magnitude of 10^2–10^3 km^2 in a resolution of 3 arcsec (~90 m). This resolution is also a prerequisite to validate model results against observed landslides from inventories (Tian et al., 2008). Yet, the corresponding computational burden jeopardizes the applicability of physically-based modeling to larger area (*e.g.*, basins≫ 10,000 km^2) (Bellugi et al., 2011; Camilo et al., 2017) and to derive necessary model parameters (Bardossy and Singh, 2008; Yao et al., 2012). In order to apply physically-based models in landslide prediction with high resolution, some computational expediency is needed in large basins.

Low-resolution but large scale hydrological models (typically applied at 1 km resolution or coarser) are widely available due to increasing availability of climate data and land surface datasets (Sun et al., 2017; Huang et al., 2019; Yao et al., 2019; van Beek et al., 2011; Wada et al., 2011; Luo et al., 2018). These models can be calibrated against observed discharge (Beck et al., 2016; Chao et al., 2018) so it captures the spatiotemporal variations across the basin. However, this coarse resolution does not fit the purpose for validation of landslide

* Corresponding author.
E-mail address: kzhang@hhu.edu.cn (K. Zhang).

https://doi.org/10.1016/j.envsoft.2019.104607
Received 14 September 2019; Received in revised form 11 December 2019; Accepted 17 December 2019
Available online 18 December 2019

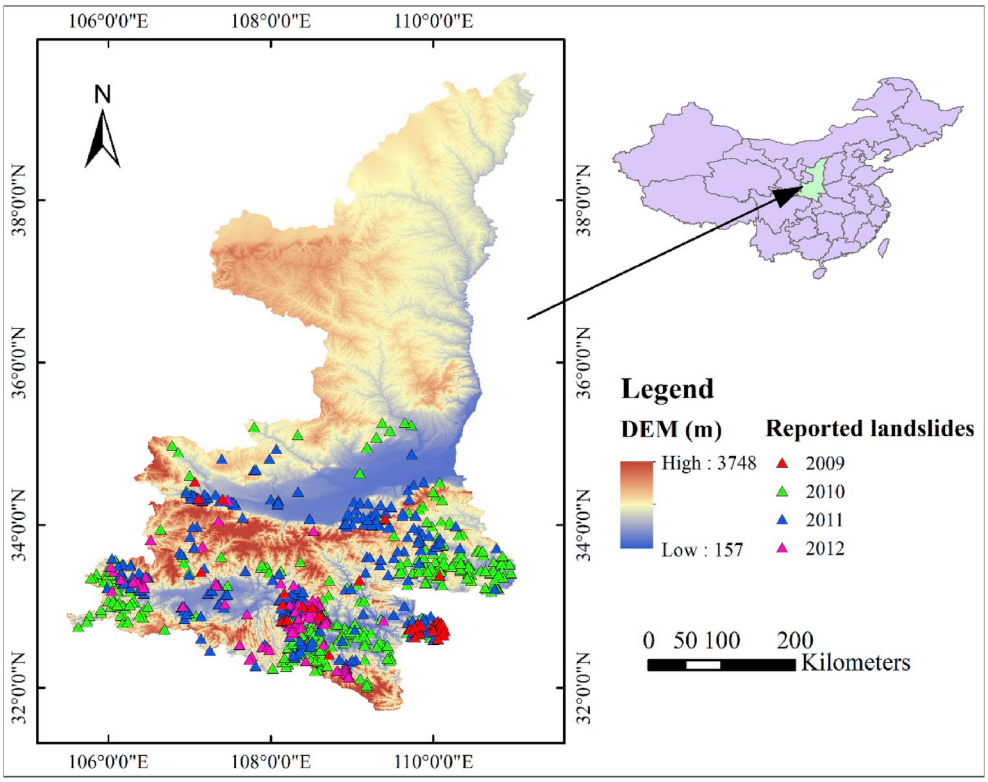

Fig. 1. Location of Shaanxi Province in the mainland of China and the reported landslides during 2009–2012.

prediction because the size of a rainfall-triggered shallow landslide event is usually only tens or hundreds m^2 (Chen et al., 2017; Zhang et al., 2018a). In this case, a downscaling method should be used in order to couple coarse-resolution hydrological models with fine-resolution slope stability models.

Soil moisture is an important component in water and energy balance, affecting subsurface flow, soil evapotranspiration, hydrological response of a catchment etc., as a linking variable between hydrological model and slope stability model (Bogaard and Greco, 2016; Zhang et al., 2019). For slope stability model, the degree of soil saturation affects ground water table response to rainfall and thereby slope stability (Talebi et al., 2007; Bogaard and Greco, 2016; Krzeminska et al., 2012). Several studies showed that topography could be a good indicator for spatial soil moisture distribution (Beaudette et al., 2013; Burt and Butcher, 1985; Sveditchnyi et al., 2003). The topographic wetness index (TWI), as one of the topographic indexes, shows a high correlation with soil moisture during wet conditions (Grayson and Western, 1998; Brocca et al., 2010). Therefore, it is reasonable to downscale the soil moisture via using TWI to link hydrological model and slope stability model under different spatial resolution.

The main objective of this study is to assess the potential of physically-based landslide hazard assessment on the scale of 100,000 km^2. In this study we use topographic information to downscale the results of the coarse-scale hydrological model to the finer resolution slope stability model in an efficient and expedient manner. The hydrological model we used is the Coupled Routing and Excess STorage (CREST) model (Wang et al., 2011), a distributed hydrological model, which has been applied at a resolution of 1 km to the Shaanxi Province

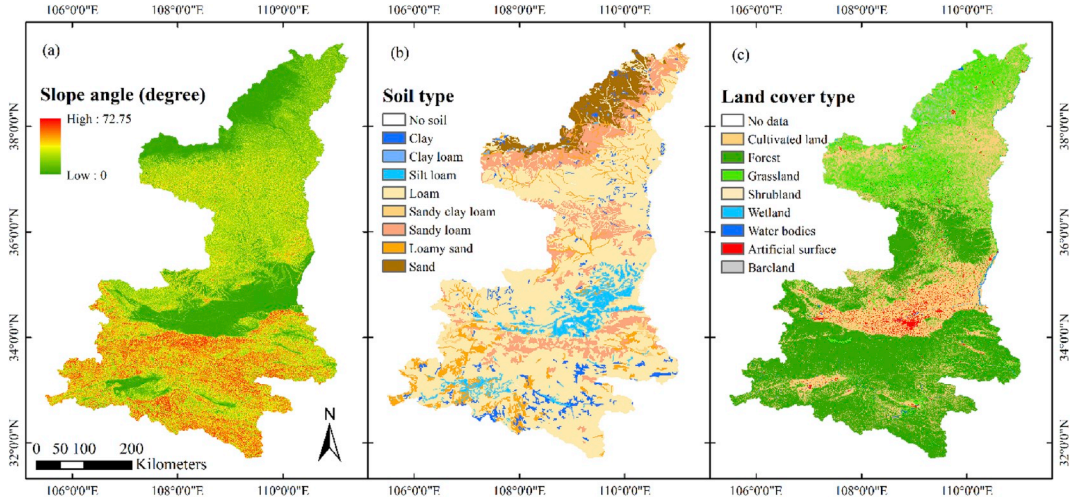

Fig. 2. Spatial maps of: a) slope angle; b) soil type and c) land cover type.

Table 1
Datasets used in this study and their pre-processing.

Variables	Sources of Datasets	Pre-processing
Rainfall	Daily rainfall data from 756 gauge stations were provided by China Meteorological Administration (CMA).	The data were interpolated into 1-km resolution via Kriging method (Krige, 1951).
Potential evapotranspiration	Global Land Data Assimilation System (GLDAS, (Rodell et al., 2004))	These data are at a spatial resolution of 0.25° and a time interval of 3 h. We interpolated it into 1-km resolution using the bi-linear method and aggregated it to daily scale.
DEM	1-km resolution DEM were from Hydrological data maps based on Shuttle Elevation Derivatives at multiple Scales (HydroSHEDS, (Lehner et al., 2006)).	The 1 km DEM of study area was extracted from the original data.
	90 m-resolution DEM were from the Geospatial Data Cloud.	The 90-m DEM of study area was extracted from the original data.
Land cover type	GlobeLand30-2010 (Chen et al., 2015)	The original 30 m dataset was resampled to 1 km and 90 m resolution for being applied in the hydrological model and slope stability model, respectively.
Soil type	Harmonized World Soil Database (HWSD) v1.2 (Wieder et al., 2014)	These data were resampled to 90-m resolution when used in slope stability model.
NDVI	Moderate Resolution Imaging Spectroradiometer (MODIS, (Jenkerson et al., 2010))	These data were resampled to 1 km using the bi-linear method.
Stable nighttime-light	Defense Meteorological Satellite Program's (DMSP) Operational Line-scan System (OLS) (Elvidge et al., 1997, 1999)	These data are at a resolution of 1 km; the data for this study area were extracted from the original data.

in Northwest China for an area of more than 200,000 km^2 for the period of 2009–2012. We downscaled the soil moisture information via TWI and land surface conditions to a finer resolution of 90 m. For the landslide assessment, we used a physically-based landslide model, namely, the SLope-Infiltration-Distributed Equilibrium (SLIDE) model (Montrasio and Valentino, 2008; He et al., 2016), which used the result of downscaled soil moisture as input variable. The results of the landslide hazard assessment are compared to classical lumped regional rainfall thresholds to quantify the possible improvement.

This article is organized as follows. It firstly describes the study area and datasets in Section 2. Then a brief introduction of hydrological model and slope stability model along with the downscaling method are described in Section 3. Section 4 presents results of our research and hence a comparison between the results and the results of landslide prediction using classic rainfall threshold is discussed in section 5. Conclusions, limitations of the research and its potential improvements are described in the end.

2. Study area and data

2.1. Description of the study area

Our study area is Shaanxi Province, located in the middle land of northwest China (Fig. 1). It situates between 105°29′ E−111°15′ E and 31°42′ N-39°35′ N with a total area of about 205,800 km^2. Elevation ranges from approximately 150 to 3800 m, which the highest elevation is in the south, followed by north and middle. Land cover is distinct from south to north: forest, cultivated land and grass land, respectively (Fig. 2b). The soil type is mainly loam in this region (Fig. 2c). The study area consists of three main climatic zones, humid zone, semi-humid zone and semi-arid zone, distributed from south to north. Average annual rainfall is 400–600 mm, 500–700 mm and 700–900 mm in northern, central and southern areas, respectively, while precipitation decreases from south to north and is significantly influenced by the mountains. In addition, rainfall has a strong seasonality in this region. Rainfall in the summer (June–August) is the greatest, accounting for 40%–60% of annual rainfall. Rainfall of the remaining seasons decreases in the order of autumn, spring and winter (Zhang et al., 2019). As rainfall is mostly concentrated in monsoon season (May–October) and in the south area with steep slopes, rainfall-triggered landslides occur frequently during these seasons in the south. There were 862 reported rainfall-triggered landslides during 2009–2012 that mainly occurred in the southern area (Fig. 1), which have resulted in 131 deaths and thousands of injuries and more than 600 million CNY directly property loss.

2.2. Datasets

The data we used in this study include rainfall, potential evapotranspiration, digital elevation model (DEM), land cover type, soil type, Normalized Difference Vegetation Index (NDVI) and stable nighttime-light data, observed discharge and landslide inventory. The DEM using in this study contains two resolutions, the 1-km resolution is 30 arcsec and the 90-m resolution is 3 arcsec. The geographic coordinate system in this study is World Geodetic System (WGS) 1984.

The detailed introduction and pre-processing of part of data are in Table 1. The rainfall and potential evapotranspiration data are the forcing data. The DEM, land cover and soil type, NDVI and stable nighttime-light data are used to calculate model parameters, such as flow duration, flow accumulation, slope angle, soil water capacity, saturated hydraulic conductivity, impervious surface area and soil cohesion, porosity, friction angle etc. The daily discharge data were used to calibrate the hydrological model and were from the Hydrological Year Books of China. We chose four discharge stations (Lueyang, Nanronghua, Shiquan, Taoyuan) that could represent the outlet of each basin to do model simulation. The landslide hazard data were from the Geological Survey Office of Department of Land and Resources of Shaanxi Province, containing landslides locations, occurrence time, and associated casualties.

3. Methods

3.1. Description of the CREST model

The CREST model (Wang et al., 2011), developed by the University of Oklahoma and NASA SERVIR project team, is a physically-based distributed hydrological model. The model simulation starts from canopy interception. After that, the rainfall, reaching soil surface, is divided into surface runoff and infiltration according to the Variable Infiltration Capacity curve (VIC), a concept originating from the Xinanjiang Model (Zhao, 1992) and later represented in the VIC model (Liang et al., 1994, 1996). The virtual multi-linear reservoir, represented as surface and subsurface water storage, is then used to calculate overland and subsurface flows, which are separated by the saturated hydraulic conductivity. A cell-to-cell routing scheme is used to simulate these flows flow to downslope cells at each time step, where it is further divided into overland flow and infiltration using VIC model. The interaction between the surface and subsurface flow is accounted for through coupling the runoff generation process and the routing scheme (Wang et al., 2011; Xue et al., 2013). The soil depth is 1.5 m and divided into three layers. A detailed description can be found in Wang (Wang et al., 2011; He et al., 2016; Xue et al., 2013).

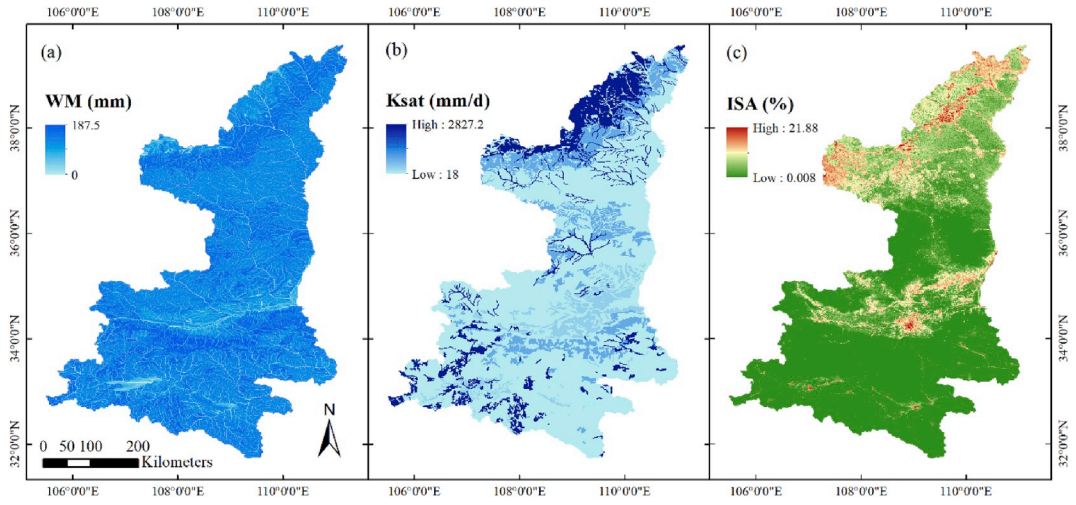

Fig. 3. Distributed parameters used in the study: a) soil water capacity, b) saturated hydraulic conductivity and c) impervious surface area.

3.2. Description of the SLIDE model

The SLIDE model, modified from two previous studies (Fredlund et al., 1996; Montrasio and Valentino, 2008), is an infinite slope stability model using a mathematical method to illustrate the rainfall-triggered landslide process. It accounts for the contribution of apparent cohesion to the shear strength of the soil and the thickness of infiltrated layer affected by rainfall-runoff processes (Liao et al., 2010). Some underlying assumption of the model are: 1) the permeability of substratum is much smaller than that of the top-soil; 2) the slope stability has a direct link to apparent cohesion, which is influenced by the degree of soil saturation (Montrasio and Valentino, 2008). The original SLIDE model considers the entire amount of rain that infiltrates into the soil, neglecting runoff and evapotranspiration, which is the disadvantage of this model. Yet, this can be fixed by using hydrological models, which takes these into account. In SLIDE model, the slope stability is represented by factor of safety, a ratio of shear strength to shear stress, expressed as follows:

$$F_s = \frac{\cot\beta \cdot \tan\Phi \cdot [\Gamma + m \cdot (n_w - 1)] + C^{'} \cdot \Omega}{\Gamma + m \cdot n_w} \quad (1)$$

where β is slope; Φ is friction angle; Γ is a function of specific gravity, porosity and degree of soil saturation; m is dimensionless thickness of the infiltrated layer and is a function of hydraulic conductivity, slope, water table depth, infiltration and degree of soil saturation, calculated at each time step; n_w is a function of porosity and degree of soil saturation; $C^{'}$ is total cohesion, including effective cohesion and apparent cohesion; Ω is a function of slope and water table depth. Detailed description can be found in Liao (Liao et al., 2010).

3.3. Model parameterization

Both the hydrological model and the slope stability model have a number of key parameters. Some of them are distributed parameters and can be derived from readily available spatial information. For the CREST model, the distributed parameters used in this study are soil water capacity, saturated hydrological conductivity and impervious surface area. For SLIDE model, most of the parameters are related to soil type (*e.g.* cohesion, porosity, unit weight and friction angle).

Soil water capacity (W_M), representing the amount of available water that each grid cell can hold, was calculated based on topography using a prior estimation method developed by Yao (Yao et al., 2012) (Fig. 3a). W_M is defined as the difference between field capacity and wilting point and it is assumed that a cell with the maximum or minimum value of *TWI* corresponds to the cell with the minimum or maximum value of W_M. A detailed description of this method can be found in Yao's research (Yao et al., 2012).

Saturated hydraulic conductivity (K_{sat}) reflects the ability of saturated soil transmitting water (Sarki et al., 2014). Recently, a global saturated hydraulic conductivity map was developed by Zhang et al. (2018b). However, the map does not completely meet the soil type map in this study area, particularly where the soil type is sand. Hence, K_{sat} was determined as specific values according to different soil types (Table 2) in this study (Fig. 3b) because it mainly relates to soil texture.

Impervious surface area (*ISA*) is the fraction of impermeable area in a grid cell, affecting rainfall infiltration and runoff generation. Generally, a grid cell with higher *ISA* generates more runoff under the same rainfall condition. *ISA* is influenced by many factors such as vegetation index and human activities. The computing procedure of *ISA* is expressed in

Table 2
Specific values of parameters for different soil types used in this study (Zhang et al., 2016; Shen and Hong, 2014).

USDA Soil Type	Soil Cohesion (kPa)	Saturated Hydraulic Conductivity (m/s)	Porosity	Friction Angle (degree)	Soil Dry Unit Weight (kN/m^3)	Field Capacity (m^3/m^3)	Wilting Point (m^3/m^3)
Silty clay	30	1.06×10^{-6}	0.49	18.5	18	0.36	0.21
Clay	40	1.31×10^{-6}	0.47	16.5	19.5	0.36	0.21
Silty clay loam	50	1.44×10^{-6}	0.48	16.5	14	0.34	0.19
Clay loam	35	2.72×10^{-6}	0.46	20	14	0.34	0.21
Silt	9	2.05×10^{-6}	0.52	26.5	16.5	0.32	0.165
Silt loam	9	2.50×10^{-6}	0.46	24	14	0.3	0.15
Sandy clay	24.5	4.31×10^{-6}	0.41	22.5	18.5	0.31	0.23
Loam	10	4.53×10^{-6}	0.43	22.5	13	0.26	0.12
Sandy clay loam	29	6.59×10^{-6}	0.39	20	15	0.33	0.175
Sandy loam	6	1.02×10^{-5}	0.4	32	15	0.23	0.1
Loamy sand	7.5	1.78×10^{-5}	0.42	28.5	20.5	0.14	0.06
Sand	5	2.44×10^{-5}	0.43	40	21	0.12	0.04

Appendix A.

Fig. 3c shows the percent of impervious surface area that mainly influenced by the vegetation cover and human activities. For most areas, especially the south covered by forest (compared with Fig. 2c), the ISA is lower while the ISA is higher in cultivated land and grass land where there are more human activities.

3.4. Downscaling method

To link the low-resolution hydrological model with the high-resolution slope stability model, a downscaling method (Sveditchnyi et al., 2003; Droesen, 2016) was applied in this study (Eq. (2)). The wetness coefficient (K_w) was proposed as a conversion parameter between TWI and soil moisture. The relation between K_w and TWI at resolution of 1 km was detected first. The concave and convex areas are distinguished. Then this relation was used to calculate K_w at the 90-m resolution via TWI_{90m}. The soil moisture was calculated through $K_{w,90m}$ and was simply fixed. The details of downscaling method can be found in Appendix B.

$$\begin{cases} SM_{90m} = (p \times TWI_{90m} + q + 0.16\cos A_{90m} + 0.09\sin A_{90m})K_{a,90m} \times SM_{1km}, & if\ Curvature \le 0 \\ SM_{90m} = (p \times TWI_{90m} + q + 0.14\cos A_{90m} + 0.10\sin A_{90m} - 0.02\cos 2A_{90m})K_{a,90m} \times SM_{1km}, & if\ Curvature > 0 \end{cases} \quad (2)$$

where SM_{90m} and SM_{1km} are soil moisture at resolution of 90 m and 1 km, respectively; p and q are two coefficients of line regression of the relation between TWI and K_w; A_{90m} is the slope aspect (degree) at 90 m-resolution; K_a is a function of slope angle and slope aspect (see Appendix B).

Table 3
Statistical metrics and gauge stations that used to evaluate model simulation.

Statistical metrics	Percent relative bias		Correlation coefficient		
	Flow duration curve (FDC)		Receiver Operating Characteristic (ROC) curve		
Stations	Longitude (°E)	Latitude (°N)	Elevation (m)	Upstream area (km^2)	River name
Lueyang	106.150	33.333	646	20793.7	Jialing River
Nanronghua	109.866	34.767	342	26302.74	Beiluo River
Shiquan	108.234	33.038	372	23622.9	Han River
Taoyuan	108.974	34.459	364	45885	Jing River

3.5. Model performance evaluation

To evaluate the model performance, several statistical metrics were applied in this study (Table 3). For CREST model, we computed the relative bias, and the Pearson correlation coefficient (Cc) for the modeled daily discharge series of four selected gauge stations. The flow duration curve, plotting discharge against the percent of time the flow was equaled or exceeded (Vogel and Fennessey, 1994), was also used to evaluate the model simulation results. In order to reduce the effect of extreme high and low flows on the calibration, we chose the discharge

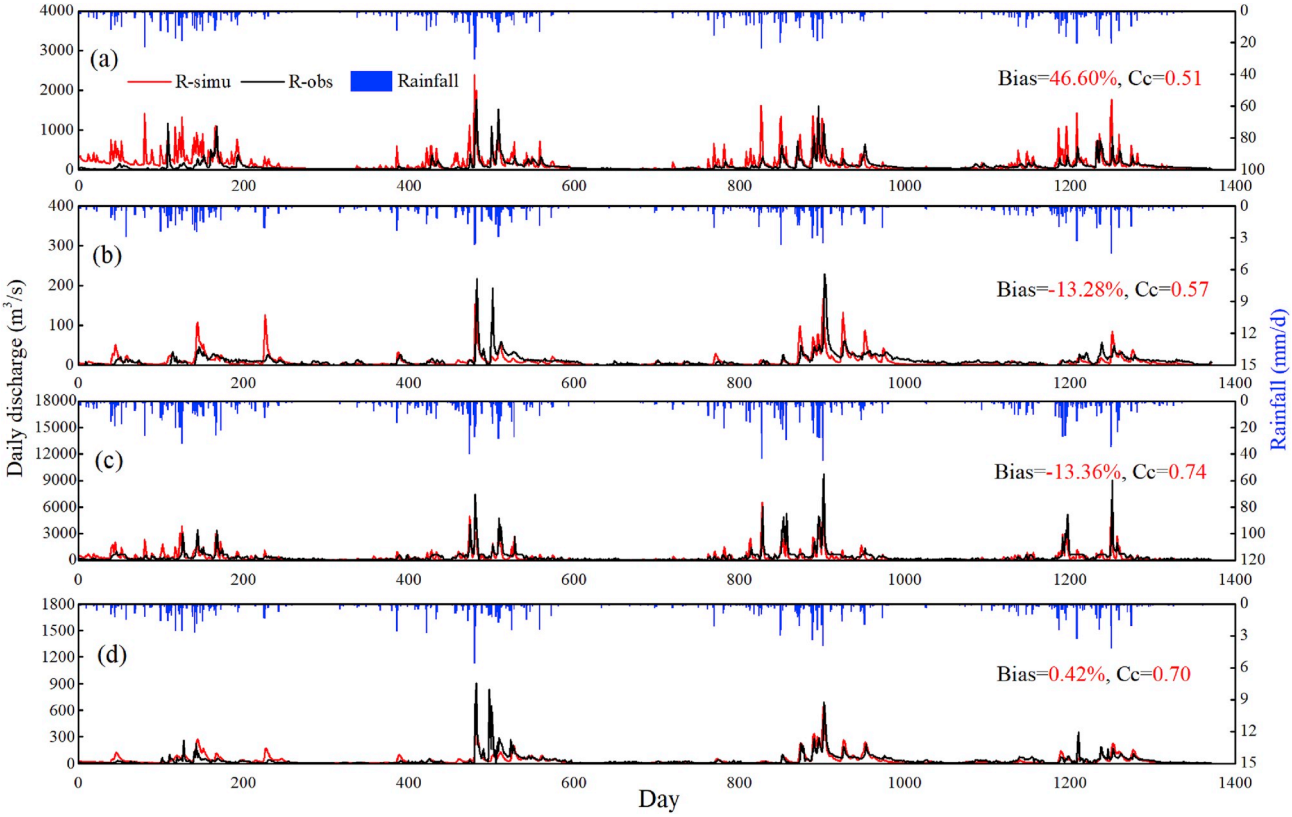

Fig. 4. Modeled and observed daily discharge and average rainfall of four gauge stations: a) Lueyang; b) Nanronghua; c) Shiquan and d) Taoyuan.

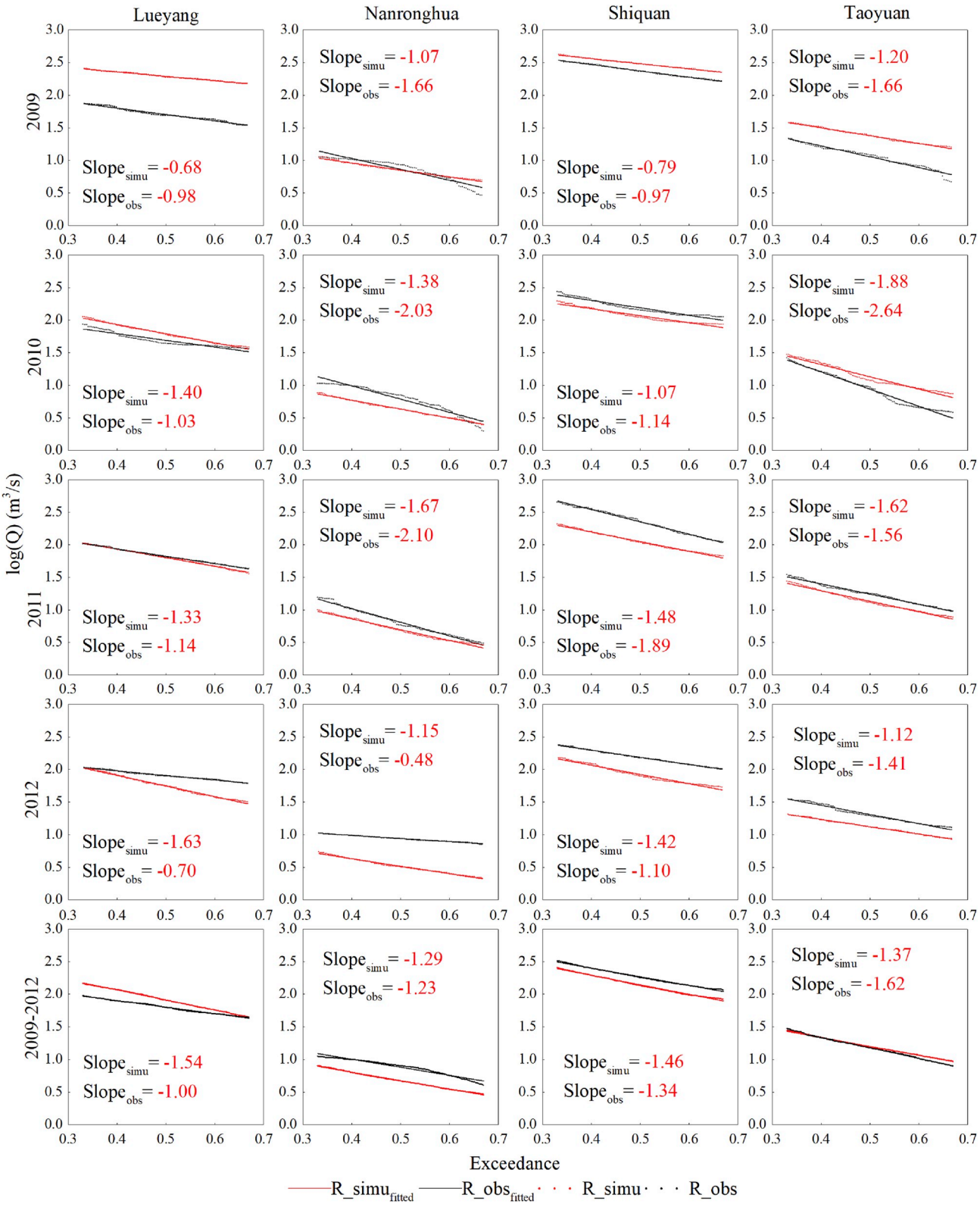

Fig. 5. Curve fitting of logarithm discharge, of which exceedance is between 0.33 and 0.67, at four-gauge stations for the period of 2009–2012.

whose exceedance is between 33 and 66% to do the curve fitting. This restriction can be justified by the fact that fitting the model with the events falling within the intermediate range can achieve a balanced performance to avoid both underestimation and overestimation. The slopes of the tendency lines for observed and simulated discharge were compared with each other by an objective function (Eq. (3)). The model simulation is good when Z is close to 0 while an *objective function* (Z) far less or greater than 0 means the model is responds too fast or too slow compared to the observed discharge, respectively.

$$Z = 1 - \frac{slope_{simu}}{slope_{obs}} \tag{3}$$

Table 4
Results of objective function (Z) of the four discharge stations for the period of 2009–2012.

Station	2009	2010	2011	2012	2009–2012
Lueyang	0.309	−0.367	−0.172	−1.326	−0.541
Nanronghua	0.354	0.323	0.204	−1.408	−0.044
Shiquan	0.191	0.059	0.217	−0.291	−0.092
Taoyuan	0.274	0.285	−0.036	0.203	0.157

where $slope_{simu}$ and $slope_{obs}$ are the slopes of the tendency lines of modeled and observed discharge, respectively.

The Receiver Operating Characteristic (ROC) curve, reflecting whether a binary classification model is good or not (Fawcett, 2006), was applied to evaluate the predictive capability of SLIDE with downscaled soil moisture to predict landslides. The binary classification model (the SLIDE model in our study) has four outcomes: true positive (TP, a landslide is predicted correctly); false positive (FP, a modeled landslide is out of landslide inventory); true negative (TN, an area is stable for both model prediction and observation); and false negative (FN, a landslide is not captured by the model). Two statistics, true positive rate (TPR, also known as sensitivity) and true negative rate (TNR, also called specificity), were further defined as follows:

$$TPR = TP / (TP + FN) \quad (4)$$

$$TNR = TN / (TN + FP) \quad (5)$$

TPR reflects the ratio that landslides were correctly predicted while *TNR* is the percentage that negative cases were correctly predicted (Begueria, 2006). High *TPR* means more landslides were captured by the model, while high *TNR* means a few modeled landslides are out of landslide database. A ROC curve consists of TPR and TNR pairs, which were calculated under different cutoff values. Factor of safety (FS) is the cutoff variable in our study. The model performs well if the ROC curve is close to the upper-right corner. The area under the curve (AUC) reflects the global accuracy of the model. The larger the AUC value, the more correct the model is in predicting landslides.

4. Results

4.1. Simulation of CREST model

The CREST model was used to simulate the hydrological processes for the period of 2009–2012 for the study area. The 2009–2010 period is used to calibrate the model, while the 2011–2012 as the validation period. In order to reduce the effect of initial conditions, the first three months were not considered in model evaluation. The model was calibrated manually. The processes of modeled and observed daily discharge for the four stations are shown in Fig. 4. The modeled discharges show generally good agreement with the observations. The relative biases are 46.60%, −13.28%, −13.36% and −0.42% while Ccs are 0.51, 0.57, 0.74 and 0.70 for Lueyang station, Nanronghua station, Shiquan station and Taoyuan station, respectively. For the modeled discharge of the first 200 days of Lueyang station, they do not meet the observations well probably because of the initial conditions, thus the bias is larger than 40% and the Cc is less than 0.6. For the other three discharge stations, the bias and Cc are all less than 20% and greater than 0.55, respectively, indicating that the CREST model performs well in these areas.

We further calculated the logarithm discharge and its exceedance of the four stations in every year to construct the FDCs between 33% and 67% exceedance probability (Fig. 5). The red and black lines are fitted exceedance curve of simulated and observed discharge, respectively. The result shows that the slopes of simulations for all the stations in the four years are generally close to those of the observations. Table 4 shows the results of the objective function for the four stations from 2009 to 2012. Most of the absolute values of the *Z* are less than 0.4, only two of them are slightly larger than 1 (for Lueyang station and Nanronghua station in 2012). However, the absolute values of average *Z* for the four stations are all less than 0.6. Besides, the average *Z* values of Nanronghua and Shiquan station are only 0.044 and 0.092, respectively, which means the simulation discharge meets the observation quite well.

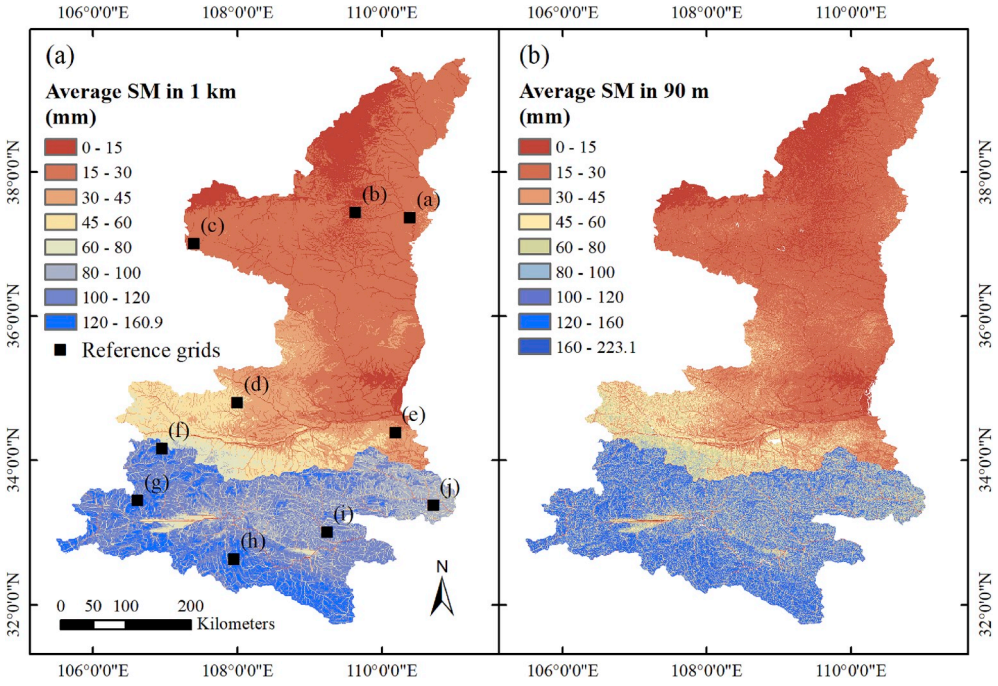

Fig. 6. Average soil moisture in spatial resolutions of a) 1 km and b) 90 m; (a)–(h) in panel a) are the selected reference grids for demonstrating the downscaling results.

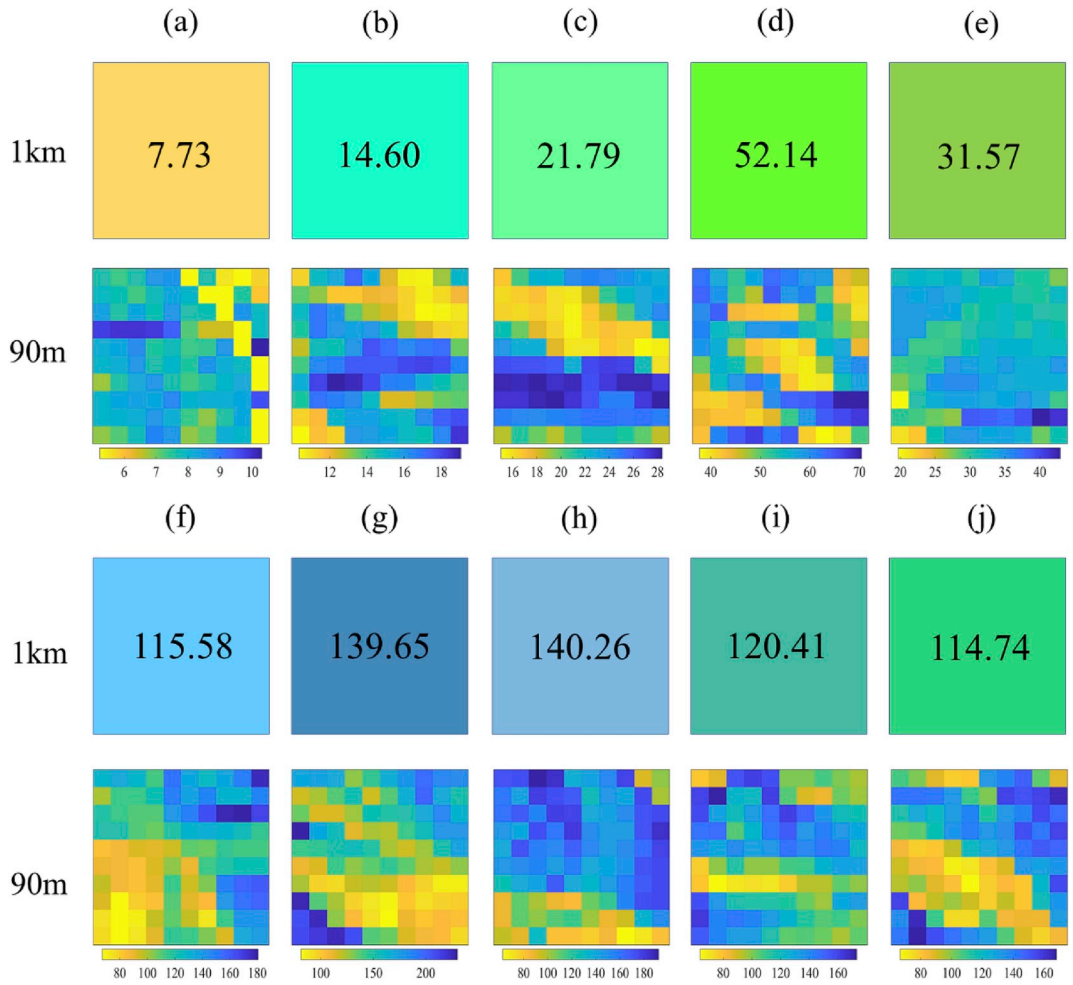

Fig. 7. Soil moisture downscaling results of ten reference grids (these grids are shown in Fig. (6)).

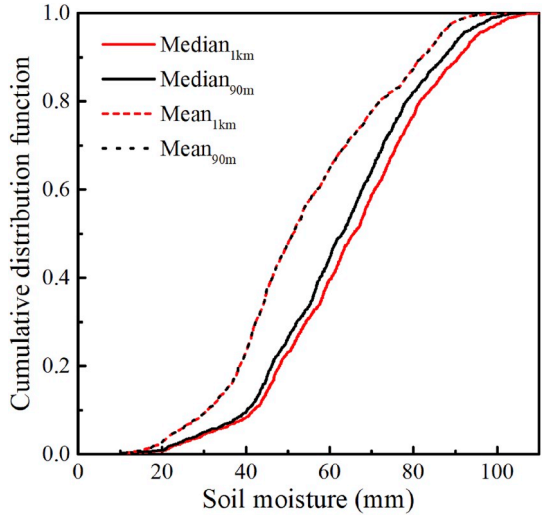

Fig. 8. Cumulative distribution functions of median and mean of soil moisture at resolution of 1 km and 90 m.

4.2. Soil moisture downscaling

The soil moisture, simulated by The CREST model, was downscaled from resolution of 1 km to resolution of 90 m before it was used in the SLIDE model. The temporal average soil moisture was calculated for resolution of 1 km and 90 m (Fig. 6). The spatial distribution of SM in 90 m is similar to that in 1 km. The SM is higher in the south and lower in the north, which is similar to the distribution of rainfall (as mentioned before, the study area is humid to arid from south to north).

We then selected 10 reference grids, which near the rivers or locate in mountains or flat plains, to evaluate the downscaling method (Fig. 6a). The downscaling results of each reference grids are shown in Fig. 7. The numbers in the first row of all the grids are the value of soil moisture in the resolution of 1 km. Panels in the second row are the downscaled soil moisture values with a resolution of 90 m. The result shows that, for all the reference grids, the average values of 90 m spatial resolution are all approximately equal to the values of corresponding grids in 1 km spatial resolution, which means that the downscaling method is reasonable and acceptable. Besides, the SM in 90 m can capture more details compared to that in 1 km according to the figure. The fine SM, obtained by the downscaling method, can be used in slope stability model to improve model performance and solve the problem of landslide prediction in large area.

We further detected the relations of median and mean value of soil moisture in every simulation day between the two spatial resolutions (Fig. 8). The mean values at the resolutions of 1 km and 90 m agree well with each other. These two cumulative lines almost coincide. Besides, the median line in resolution of 90 m is above that in resolution of 1 km and closer to the mean line, meaning that the soil moisture is more detailed and close to the real value after downscaling because although the median can reduce the effect from the extreme value, it neglects the changes of part of the data and these changes can be considered by the mean value.

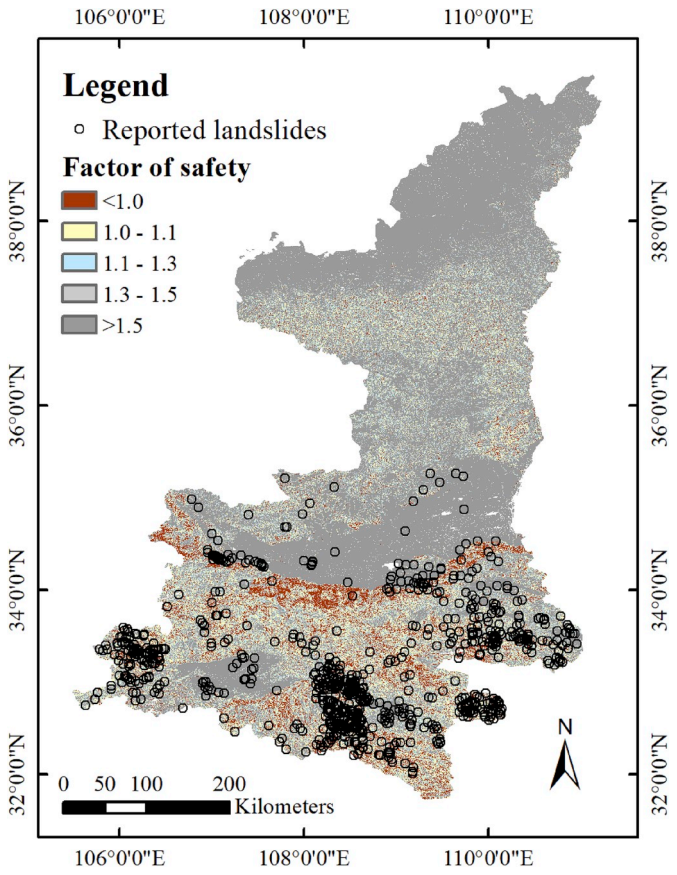

Fig. 9. The minimum factor of safety of the study area during the modeled period.

4.3. Landslide prediction

The SLIDE model was implemented to predict landslides. Fig. 9 shows the minimum FS of the whole region during the four years in the resolution of 90 m. The TPR value of the modeled results is 66.9% while the TNR value is 99.7%; these results indicate that the SLIDE model has a high accuracy in predicting landslide events and a very high accuracy in predicting stable grids. The reported landslides were concentrated in the southern area and a few in the central part where the FS is lower than 1 in most of the grid cells. Although there are no reported landslides in some places where the FS is less than 1, the model captures most of the reported landslides. Besides, the south area has the concentrated mountains and rainfall, which is the cause of landslides that concentrate in this area.

The mean of soil moisture and the percentage of unstable grids are shown in Fig. 10. The black line is the mean of soil moisture while the blue line is the mean of soil moisture which grids locate the area that the DEM is higher than 500 m and the slope angle larger than 10°. Generally, the percent of unstable grids increases with the increasing soil moisture. This suggests that there is a strong relation between soil moisture and slope stability. Besides, the statistical analysis shows that the Cc of blue line and red line is larger than that of black line and red line which means the changes of soil moisture in high elevation and steep slope has more significant effects on slope stability.

We further conducted the ROC analysis, which can reflect the performance of the SLIDE model. The whole area is too large and contains more than 28,000,000 grid cells in resolution of 90 m. In order to analyze more efficiently, we randomly chose 100,000 grid cells that had no reported landslide events and gave each of them a date randomly. To make these selected grid cells represent the whole study region well, we made sure that any two of the 100,000 grid cells are separated by at least 7 grid cells. For each of the randomly chosen grid cells (including these with reported landslide events), the grid cells that are close to it within three grids were selected. The minimum FS of these grids was then obtained during the model day-by-day simulation. The TPR and TNR pairs were calculated using the confusion matrix. The ROC curve of the SLIDE model is shown in Fig. 12. The curve is the close to the upper-right corner. The AUC of the SLIDE model (also known as the global accuracy) is 0.972 while the TPR is 0.669, meaning that the model has high global accuracy and true positive rate. In addition, the TNR of the model is 0.997, indicating that the SLIDE model has skill also to delineate the stable area.

5. Discussion

In this study, we coupled the low-resolution hydrological model CREST with the high-resolution slope stability model SLIDE using a

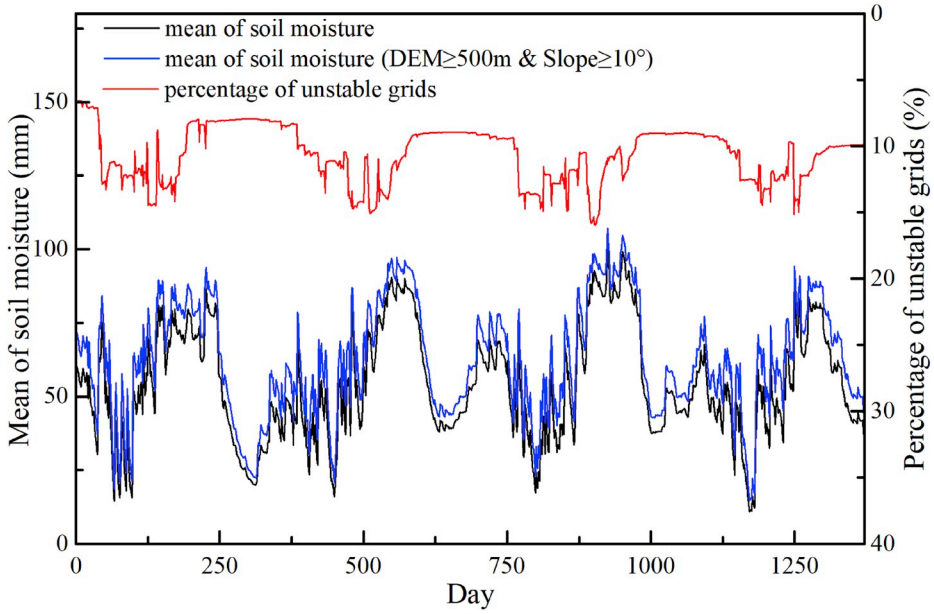

Fig. 10. Time series of mean value of soil moisture and percentage of unstable grids over the whole region.

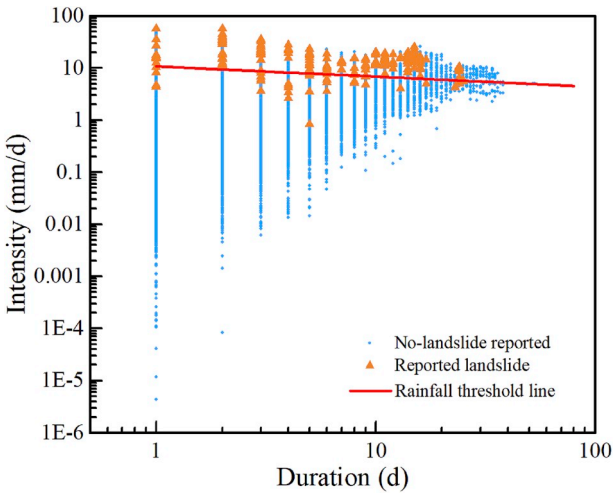

Fig. 11. Threshold line of the ID model for distinguishing the reported slided and non-slided grids.

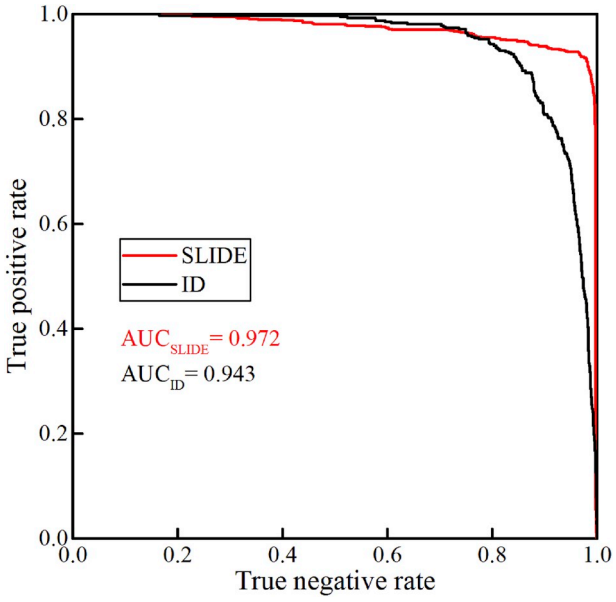

Fig. 12. ROC curves of the SLIDE model and the ID model.

spatial downscaling method for soil moisture, which is a connection variable between these two physically-based distributed models.

High-resolution hydrological modeling has a better representation of spatial heterogeneity of land surface attributes (*e.g.* topography, soil, and land cover) (Wood et al., 2011), however, it is difficult and inefficient, sometimes infeasible to apply these models with a very fine resolution in a large area, especially for the CREST model (*e.g.* 90 m resolution in this study). Meanwhile, modeling in a high-resolution requires large, massive computer resources (Wood et al., 2011; Kumar et al., 2006), which is very costly and time consuming. Kollet et al. (2010) presented a parallel scaling study that couples groundwater and land-surface modeling system by using more than 16,000 processors, and it takes about 200 min for a 10 days simulation. Besides, high resolution is not necessary for hydrological models to have improved performance because of the quality of the data (Li and Wong, 2010). Horritt and Bates (2001) found that the hydrological model reaches the best performance at a spatial resolution of 100 m, and no improvement with increasing resolution. This study was implemented in a 60 km river channel, which is substantially smaller than the study area in our research. Hence, the hydrological model with a resolution of 1 km is suitable and effective in regional scale, *e.g.* our study area. In addition, it is difficult to obtain the parameters of hydrological models in a very high spatial resolution. For landslide prediction, it shows that the model has high global accuracy and good performance. Due to the computational load, it is impossible to model in a finer resolution (i.e. 30 m or 10 m) over such a large region, we did not detect whether the model performance will be better or not in the resolution of 30 m. In fact, it has been pointed that too high resolution may not lead to better results (Tian et al., 2008; Arnone et al., 2016). Furthermore, it should be noted that at very fine resolutions, errors and incompleteness of the landslide inventory starts to have more significant effects on landslide prediction (Arnone et al., 2016). The method proposed in this study can be used in other large regions because of the wide applicability and feasibility of the CREST model and SLIDE model. This coupling method also makes it possible to develop landslide prediction system on a global scale.

The main objective of this study is landslide assessment. In order to evaluate the performance of the SLIDE model for landslide prediction, we conducted the classical ID (Intensity-Duration) threshold method (Bogaard and Greco, 2018; Peruccacci et al., 2017; Huang et al., 2015; Melillo et al., 2018) to compare the results of the two methods. The intensity and duration of rainfall events for each random grid cell and reported landslides were calculated first. A rainfall event is defined as the continuous rainfall or discontinued rains with the non-rain intermittent periods less than or equal to 1 days. Then we chose half of the reported landslides and half of the random grid cells as the model calibrating dataset. The rest of the dataset is for validating. The intensity and duration of calibrating dataset were plotted on a log-log graph (Fig. 11). Curve fitting by linear regression of these scatters was implemented afterwards. We adjusted the line by changing its intercept to make sure that 90% of the total grids are predicted correctly by the ID model (Eq. (6)). The ID model was validated lastly. For a reported landslide or a no-landslide grid, it is predicted correctly if it locates above the line or below the line, respectively.

$$\log_{10} I = 1.291 - 0.198 \times \log_{10} D \quad (6)$$

where I is rainfall intensity in mm/d; D is rainfall duration in day (d).

The three metrics, TPR, TNR and AUC, are 0.669, 0.997 and 0.972 for the SLIDE model, respectively, while they are 0.907, 0.852 and 0.943 for the ID model, respectively. The ID model has higher TPR than the SLIDE model, which has higher TNR. However, if we adjusted the threshold line and changed the TNR of the ID model to 0.997, which equals to that of the SLIDE model, the TPR of the ID model will be only 0.132, which is far less than that of the SLIDE model. Besides, the ROC curve of the SLIDE model has higher AUC value and is closer to the upper-right corner than that of the ID model (Fig. 12). These results suggest that, although it has lower TPR, the SLIDE model is more robust than the ID model in landslide prediction which maybe because it is a physically-based distributed model that the soil and the topographic attributes can be better considered in model simulation. In addition, it should be noticed that the reported landslides mainly occurred in the southern mountain area, which is mainly covered by forest. Hence, some landslide events may not be monitored or reported.

6. Conclusions

This study aims to predict landslides in a very large region by coupling a low-resolution hydrological model with a high-resolution slope stability model. The soil moisture is the coupling variable, which should be downscaled to use in the slope stability model. The topographic wetness index is the downscaling parameter linking the coarser-resolution soil moisture with the finer one.

The CREST model and the SLIDE model were applied in this study. Both of the two models performed well: the CREST model simulated the hydrological processes good while the SLIDE model predicted landslides

more robustly compared to the result of a regional threshold approach. These results indicate that the model and downscaling methods applied in this study are useful for landslide prediction in large regions. Yet, these methods can be improved through more data sets and more accurate initial conditions. For parameters, they can be calibrated and validated by field experiments; for soil moisture downscaling, the field observation data could be useful for validation. It is a massive work collecting these data in such large area. However, with technology developing, these problems could be solved and there will be more efficient and accurate methods for landslide hazard assessment over large regions (*e.g.* continental scale and global scale).

Author contributions

KZ, TB, LPHvB and SW designed this study; KZ and SW set up the models; SW,TB, and KZ conducted this study; SW and KZ wrote the manuscript; SW, KZ, TB, LPHvB and XT contributed to the discussion and revision.

Declaration of competing interest

The authors declare that they have no known competing financial interests or personal relationships that could have appeared to influence the work reported in this paper.

Acknowledgement

The first author is grateful to PhD candidate Changrang Zhou for her inspiring idea about algorithm coding. This study is supported by the National Key Research and Development Program of China (2018YFC1508101, 2016YFC0402701), National Natural Science Foundation of China (51879067), Natural Science Foundation of Jiangsu Province (BK20180022), Six Talent Peaks Project in Jiangsu Province (NY-004), and Fundamental Research Funds for the Central Universities of China (2018B42914, 2018B04714). SW was also supported by the China Scholarship Council for his joint PhD study in the Delft University of Technology with the project reference number of 201806710078.

Appendix A

The ISA is affected by vegetation cover and human activities. Human settlement index (HSI) is an index that reflects human activities and was developed by Lu et al. (2008). The vegetation index was also considered, as expressed in the following equation:

$$HSI = \frac{(1 - NDVI_{max}) + OLS_{nor}}{(1 - OLS_{nor}) + NDVI_{max} + OLS_{nor} \times NDVI_{max}} \tag{A.1}$$

where $NDVI_{max}$ is the maximum NDVI value during April and October from 2009 to 2012, this is to reduce the impact of bare soil when using vegetation index; OLS_{nor} is the normalized value of the DMSP-OLS DN image, whose original value is between 0 and 63.

The DMSP-OLS stable nighttime-light reflects the urbanization of an area. The higher value of stable light is, the higher urbanization is. In order to match the data range between $NDVI_{max}$ and DMSP-OLS data, the DN value is normalized ranging from 0 to 1, as expressed following:

$$OLS_{nor} = \frac{OLS - OLS_{min}}{OLS_{max} - OLS_{min}} \tag{A.2}$$

where OLS_{max} and OLS_{min} are the maximum and minimum values in DMSP-OLS dataset.

In general, a grid cell with a higher vegetation index and a lower stable nighttime-light has a lower impervious area. In order to connect *ISA* with *HSI*, a simple function was established as follows:

$$ISA = p + q \times \ln HSI \tag{A.3}$$

where p and q are two coefficients and determined through model simulation.

Appendix B

Generally, the original $K_{w,1km}$ (Fig. B.1a) can be simply calculated by dividing soil moisture by its spatial mean value (Eq. (B.1)) (Droesen, 2016). In fact, the original K_w was calculated through the ratio of soil moisture to the mean value of observed soil moisture in the study implemented by Droesen (2016). However, for such a large region investigated in this study, we cannot obtain the gauge values. Therefore, we simply calculated the K_w values by dividing soil moisture by its spatial mean value. The coefficient c was then computed according to whether the curvature is less than 0 or not (for concave or straight area, the curvature is less than or equal to 0; for convex area, the curvature is greater than 0) (Eq. (B.2)).

$$K_{w,1km} = SM_{1km} \Big/ \overline{SM_{1km}} \tag{B.1}$$

$$\begin{cases} c_{1km} = \dfrac{K_{w,1km}}{K_{a,1km}} - 0.16\cos A_{1km} - 0.09\sin A_{1km}, & if\ Curvature \le 0 \\ c_{1km} = \dfrac{K_{w,1km}}{K_{a,1km}} - 0.14\cos A_{1km} - 0.10\sin A_{1km} + 0.02\cos 2A_{1km}, & if\ Curvature > 0 \end{cases} \tag{B.2}$$

where SM_{1km} is the average value of soil moisture in time series and $\overline{SM_{1km}}$ is its spatial mean value; A is slope aspect (degrees); K_a is a function of slope angle and slope aspect, as expressed below:

$$K_a = (1 - k_e\alpha) / (1 - k_e\alpha_0) \tag{B.3}$$

where α is slope angle (degrees); α_0 is average slope angle; k_e is a coefficient dependent on the aspect (for northern aspect $k_e = -0.01$, for eastern aspect $k_e = 0.002$, for southern aspect $k_e = 0.005$, and for western aspect $k_e = -0.003$ (Romanova, 1971)).

Then a relation between c_{1km} and TWI_{1km} was built by fitting their scatters where a linear regression method was applied (Eq. (B.4)). This relation was used to calculate c_{90m} via TWI_{90m}. After that, $K_{w,90m}$ (Fig. B.1b) can be calculated through c_{90m} (Eq. (B.5)).

$$c_{1km} = p \times TWI_{1km} + q \tag{B.4}$$

$$\begin{cases} K_{w,90m} = (p \times TWI_{90m} + q + 0.16\cos A_{90m} + 0.09\sin A_{90m})K_{a,90m}, & if\ Curvature \le 0 \\ K_{w,90m} = (p \times TWI_{90m} + q + 0.14\cos A_{90m} + 0.10\sin A_{90m} - 0.02\cos 2A_{90m})K_{a,90m}, & if\ Curvature > 0 \end{cases} \tag{B.5}$$

where p and q are two coefficients of linear regression.

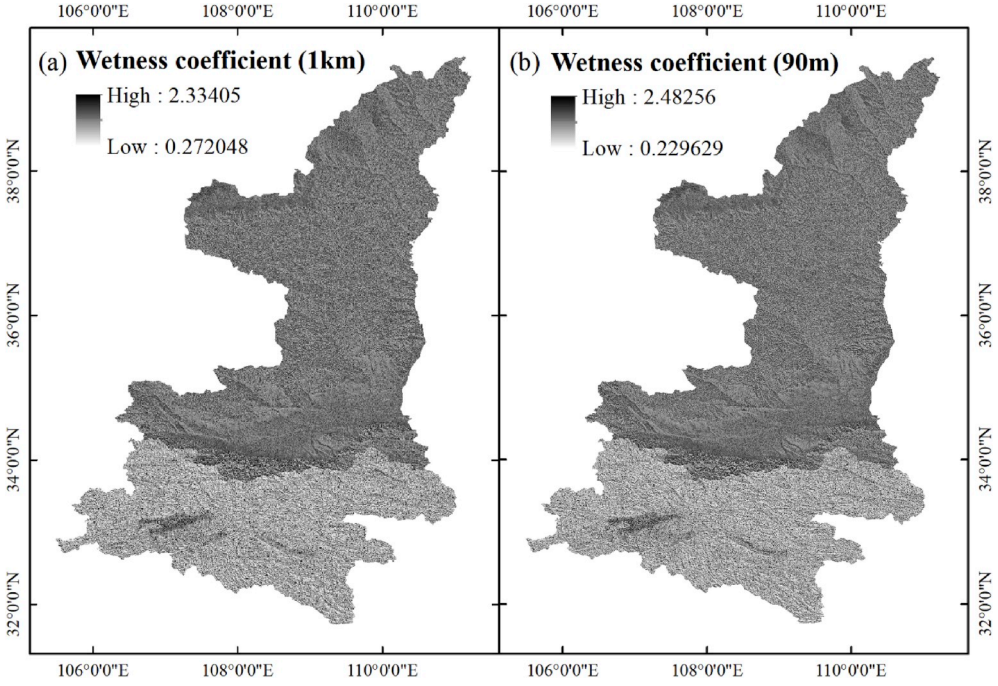

Fig. B.1. Maps of the wetness coefficient at the resolutions of 1 km and 90 m.

Finally, the SM in 90 m resolution was computed through Eq. (B.6) and was simply calibrated by forcing the average value of SM_{90m} equal to SM_{1km} in the corresponding grid cell (Eq. (B.7)) at each time step.

$$SM_{i,m,90m} = K_{w,i,m,90m} \times SM_{m,1km} \tag{B.6}$$

$$\frac{1}{n}\sum_{i}^{n} SM_{i,m,90m} = SM_{m,1km} \tag{B.7}$$

where $SM_{i,m,90m}$ and $K_{w,i,m,90m}$ are the soil moisture and wetness coefficient in i^{th} finer grid of m^{th} coarser grid; $SM_{m,1km}$ is the soil moisture in the m^{th} coarser grid; n is the total number of finer grid cells in m^{th} coarser grid.

Data availability. Rainfall data were provided by China Meteorological Administration (http://data.cma.cn). The potential evapotranspiration data were provided by Global Land Data Assimilation System (GLDAS, https://ldas.gsfc.nasa.gov/gldas/GLDASdownload.php). The DEM data in resolution of 90 m were provided by Geospatial Data Cloud site, Computer Network Information Center, Chinese Academy of Sciences (http://www.gscloud.cn). The DEM data in resolution of 1 km were provided by HydroSHEDS (https://hydrosheds.org/pages/availability). The land cover data were derived from GlobeLand30-2010, which is a product of global land cover at a spatial resolution of 30 m derived from remote-sensing images in 2010 (http://www.globeland30.cn). The soil data are from the Harmonized World Soil Database (HWSD) v1.2 (https://daac.ornl.gov/SOILS/guides/HWSD.html, Soil data, 2017). The landslide hazard data was from geological survey office of Department of Land and Resources of Shaanxi Province. The NDVI data were provided by Moderate Resolution Imaging Spectroradiometer (MODIS) and were downloaded from USGS (United State Geographic Survey) website (https://earthexplorer.usgs.gov). The Defense Meteorological Satellite Program's (DMSP) Operational Line-scan System (OLS) nighttime-light data with 1 km spatial resolution was downloaded from the National Geophysical Data Center (NGDC, http://www.ngdc.noaa.gov/dmsp/global_composites_v2.html).

Appendix C. Supplementary data

Supplementary data to this article can be found online at https://doi.org/10.1016/j.envsoft.2019.104607.

References

Bellugi, D., Dietrich, W.E., Stock, J., McKean, J., Kazian, B., Hargrove, P., 2011. Spatially explicit shallow landslide susceptibility mapping over large areas. In: Genevois, R., Hamilton, D.L., Prestininzi, A. (Eds.), Proceedings of the 5th International Conference on Debris-Flow Hazards Mitigation: Mechanics, Prediction and Assessment; Padua, Italy; June 7-11, 2011. Casa Editrice Universita La Sapienza, Rome, Italy, pp. 759–768. Italian Journal of Engineering Geology and Environment-Book, 759-768.

Alvioli, M., Baum, R.L., 2016. Parallelization of the TRIGRS model for rainfall-induced landslides using the message passing interface. Environ. Model. Softw 81, 122–135. https://doi.org/10.1016/j.envsoft.2016.04.002.

An, H., Viet, T.T., Lee, G., Kim, Y., Kim, M., Noh, S., Noh, J., 2016. Development of time-variant landslide-prediction software considering three-dimensional subsurface unsaturated flow. Environ. Model. Softw 85, 172–183. https://doi.org/10.1016/j.envsoft.2016.08.009.

Arnone, E., Francipane, A., Scarbaci, A., Puglisi, C., Noto, L.V., 2016. Effect of raster resolution and polygon-conversion algorithm on landslide susceptibility mapping. Environ. Model. Softw 84, 467–481. https://doi.org/10.1016/j.envsoft.2016.07.016.

Bardossy, A., Singh, S.K., 2008. Robust estimation of hydrological model parameters. Hydrol. Earth Syst. Sci. 12, 1273–1283. https://doi.org/10.5194/hess-12-1273-2008.

Beaudette, D.E., Dahlgren, R.A., O'Geen, A.T., 2013. Terrain-shape indices for modeling soil moisture dynamics. Soil Sci. Soc. Am. J. 77, 1696–1710. https://doi.org/10.2136/sssaj2013.02.0048.

Beck, H.E., van Dijk, A.I.J.M., de Roo, A., Miralles, D.G., McVicar, T.R., Schellekens, J., Bruijnzeel, L.A., 2016. Global-scale regionalization of hydrologic model parameters. Water Resour. Res. 52, 3599–3622. https://doi.org/10.1002/2015wr018247.

Begueria, S., 2006. Validation and evaluation of predictive models in hazard assessment and risk management. Nat. Hazards 37, 315–329. https://doi.org/10.1007/s11069-005-5182-6.

Bogaard, T.A., Greco, R., 2016. Landslide hydrology: from hydrology to pore pressure. Wires Water 3, 439–459. https://doi.org/10.1002/wat2.1126.

Bogaard, T., Greco, R., 2018. Invited perspectives: hydrological perspectives on precipitation intensity-duration thresholds for landslide initiation: proposing hydro-meteorological thresholds. Nat. Hazard Earth Sys. 18, 31–39. https://doi.org/10.5194/nhess-18-31-2018.

Brocca, L., Melone, F., Moramarco, T., Morbidelli, R., 2010. Spatial-temporal variability of soil moisture and its estimation across scales. Water Resour. Res. 46 https://doi.org/10.1029/2009wr008016. Artn W02516.

Burt, T.P., Butcher, D.P., 1985. Topographic controls of soil-moisture distributions. J. Soil Sci. 36, 469–486. https://doi.org/10.1111/j.1365-2389.1985.tb00351.x.

Caine, N., 1980. The rainfall intensity - duration control of shallow landslides and debris flows. Geogr. Ann. 62, 23–27. https://doi.org/10.2307/520449.

Camilo, D.C., Lombardo, L., Mai, P.M., Dou, J., Huser, R., 2017. Handling high predictor dimensionality in slope-unit-based landslide susceptibility models through LASSO-penalized Generalized Linear Model. Environ. Model. Softw 97, 145–156. https://doi.org/10.1016/j.envsoft.2017.08.003.

Chao, L., Zhang, K., Li, Z., Wang, J., Yao, C., Li, Q., 2018. Applicability assessment of the CASCade Two Dimensional SEDiment (CASC2D-SED) distributed hydrological model for flood forecasting across four typical medium and small watersheds in China. Journal of Flood Risk Management, e12518.

Chen, J., Chen, J., Liao, A., Cao, X., Chen, L., Chen, X., He, C., Han, G., Peng, S., Lu, M., 2015. Global land cover mapping at 30 m resolution: a POK-based operational approach. ISPRS J. Photogrammetry Remote Sens. 103, 7–27.

Chen, C.W., Oguchi, T., Hayakawa, Y.S., Saito, H., Chen, H., 2017. Relationship between landslide size and rainfall conditions in Taiwan. Landslides 14, 1235–1240. https://doi.org/10.1007/s10346-016-0790-7.

Droesen, J.M., 2016. Downscaling Soil Moisture Using Topography: the Evaluation and Optimisation of a Downscaling Approach.

Elvidge, C.D., Baugh, K.E., Kihn, E.A., Kroehl, H.W., Davis, E.R., 1997. Mapping city lights with nighttime data from the DMSP operational linescan system. Photogramm. Eng. Remote Sens. 63, 727–734.

Elvidge, C.D., Baugh, K.E., Dietz, J.B., Bland, T., Sutton, P.C., Kroehl, H.W., 1999. Radiance calibration of DMSP-OLS low-light imaging data of human settlements. Remote Sens. Environ. 68, 77–88. https://doi.org/10.1016/S0034-4257(98)00098-4.

Fawcett, T., 2006. An introduction to ROC analysis. Pattern Recognit. Lett. 27, 861–874.

Fookes, P.G., 1997. Geology for engineers: the geological model, prediction and performance. Q. J. Eng. Geol. 30, 293–424. https://doi.org/10.1144/Gsl.Qjeg.1997.030.P4.02.

Fredlund, D.G., Xing, A.Q., Fredlund, M.D., Barbour, S.L., 1996. The relationship of the unsaturated soil shear strength to the soil-water characteristic curve. Can. Geotech. J. 33, 440–448. https://doi.org/10.1139/t96-065.

Glade, T., Crozier, M., Smith, P., 2000. Applying probability determination to refine landslide-triggering rainfall thresholds using an empirical "Antecedent Daily Rainfall Model. Pure Appl. Geophys. 157, 1059–1079. https://doi.org/10.1007/s000240050017.

Godt, J.W., Baum, R.L., Lu, N., 2009. Landsliding in partially saturated materials. Geophys. Res. Lett. 36 https://doi.org/10.1029/2008gl035996. Artn L02403.

Grayson, R.B., Western, A.W., 1998. Towards areal estimation of soil water content from point measurements: time and space stability of mean response. J. Hydrol. 207, 68–82. https://doi.org/10.1016/S0022-1694(98)00096-1.

Griffiths, J.S., 2002. Mapping in Engineering Geology.

Griffiths, J.S., Edwards, R.J., 2001. The development of land surface evaluation for engineering practice. Geological Society, London, Engineering Geology Special Publications 18, 3–9.

Guzzetti, F., Cardinali, M., Reichenbach, P., Carrara, A., 2000. Comparing landslide maps: a case study in the Upper Tiber River basin, central Italy. Environ. Manag. 25, 247–263. https://doi.org/10.1007/s002679910020.

Guzzetti, F., Peruccacci, S., Rossi, M., Stark, C.P., 2007. Rainfall thresholds for the initiation of landslides in central and southern Europe. Meteorol. Atmos. Phys. 98, 239–267. https://doi.org/10.1007/s00703-007-0262-7.

Guzzetti, F., Peruccacci, S., Rossi, M., Stark, C.P., 2008. The rainfall intensity-duration control of shallow landslides and debris flows: an update. Landslides 5, 3–17. https://doi.org/10.1007/s10346-007-0112-1.

He, X.G., Hong, Y., Vergara, H., Zhang, K., Kirstetter, P.E., Gourley, J.J., Zhang, Y., Qiao, G., Liu, C., 2016. Development of a coupled hydrological-geotechnical framework for rainfall-induced landslides prediction. J. Hydrol. 543, 395–405. https://doi.org/10.1016/j.jhydrol.2016.10.016.

Hong, Y., Adler, R., Huffman, G., 2006. Evaluation of the potential of NASA multi-satellite precipitation analysis in global landslide hazard assessment. Geophys. Res. Lett. 33 https://doi.org/10.1029/2006gl028010.

Hong, H.Y., Chen, W., Xu, C., Youssef, A.M., Pradhan, B., Bui, D.T., 2017. Rainfall-induced landslide susceptibility assessment at the Chongren area (China) using frequency ratio, certainty factor, and index of entropy. Geocarto Int. 32, 139–154. https://doi.org/10.1080/10106049.2015.1130086.

Horritt, M.S., Bates, P.D., 2001. Effects of spatial resolution on a raster based model of flood flow. J. Hydrol. 253, 239–249. https://doi.org/10.1016/S0022-1694(01)00490-5.

Huang, Y., Bárdossy, A., Zhang, K., 2019. Sensitivity of hydrological model to the temporal and spatial resolutions of rainfall input. Hydrol. Earth Syst. Sci. Discuss. 23, 2647–2663. https://doi.org/10.5194/hess-23-2647-2019.

Huang, J., Ju, N.P., Liao, Y.J., Liu, D.D., 2015. Determination of rainfall thresholds for shallow landslides by a probabilistic and empirical method. Nat. Hazard Earth Sys. 15, 2715–2723. https://doi.org/10.5194/nhess-15-2715-2015.

Jenkerson, C.B., Maiersperger, T., Schmidt, G., 2010. eMODIS: a user-friendly data source. US Geological Survey2331- 1258.

Kollet, S.J., Maxwell, R.M., Woodward, C.S., Smith, S., Vanderborght, J., Vereecken, H., Simmer, C., 2010. Proof of concept of regional scale hydrologic simulations at hydrologic resolution utilizing massively parallel computer resources. Water Resour. Res. 46 https://doi.org/10.1029/2009wr008730. Artn W04201.

Krige, D.G., 1951. A Statistical Approach to Some Mine Valuation and Allied Problems on the Witwatersrand. By DG Krige, University of the Witwatersrand.

Krzeminska, D.M., Bogaard, T.A., van Asch, T.W.J., van Beek, L.P.H., 2012. A conceptual model of the hydrological influence of fissures on landslide activity. Hydrol. Earth Syst. Sci. 16, 1561–1576. https://doi.org/10.5194/hess-16-1561-2012.

Kumar, S.V., Peters-Lidard, C.D., Tian, Y., Houser, P.R., Geiger, J., Olden, S., Lighty, L., Eastman, J.L., Doty, B., Dirmeyer, P., Adams, J., Mitchell, K., Wood, E.F., Sheffield, J., 2006. Land information system: an interoperable framework for high resolution land surface modeling. Environ. Model. Softw 21, 1402–1415. https://doi.org/10.1016/j.envsoft.2005.07.004.

Lehner, B., Verdin, K., Jarvis, A., 2006. HydroSHEDS Technical Documentation, Version 1.0. World Wildlife Fund US, Washington, DC, pp. 1–27.

Li, J., Wong, D.W.S., 2010. Effects of DEM sources on hydrologic applications. Comput Environ Urban 34, 251–261. https://doi.org/10.1016/j.compenvurbsys.2009.11.002.

Liang, X., Lettenmaier, D.P., Wood, E.F., Burges, S.J., 1994. A simple hydrologically based model of land-surface water and energy fluxes for general-circulation models. J Geophys Res-Atmos 99, 14415–14428. https://doi.org/10.1029/94jd00483.

Liang, X., Lettenmaier, D.P., Wood, E.F., 1996. One-dimensional statistical dynamic representation of subgrid spatial variability of precipitation in the two-layer variable infiltration capacity model. J Geophys Res-Atmos 101, 21403–21422. https://doi.org/10.1029/96jd01448.

Liao, Z.H., Hong, Y., Wang, J., Fukuoka, H., Sassa, K., Karnawati, D., Fathani, F., 2010. Prototyping an experimental early warning system for rainfall-induced landslides in Indonesia using satellite remote sensing and geospatial datasets. Landslides 7, 317–324. https://doi.org/10.1007/s10346-010-0219-7.

Lu, D.S., Tian, H.Q., Zhou, G.M., Ge, H.L., 2008. Regional mapping of human settlements in southeastern China with multisensor remotely sensed data. Remote Sens. Environ. 112, 3668–3679. https://doi.org/10.1016/j.rse.2008.05.009.

Luo, P., Zhou, M., Deng, H., Lyu, J., Cao, W., Takara, K., Nover, D., Schladow, S.G., 2018. Impact of forest maintenance on water shortages: Hydrologic modeling and effects of climate change. Science of the Total Environment 615, 1355–1363. https://doi.org/10.1016/j.scitotenv.2017.09.044.

Melillo, M., Brunetti, M.T., Peruccacci, S., Gariano, S.L., Roccati, A., Guzzetti, F., 2018. A tool for the automatic calculation of rainfall thresholds for landslide occurrence. Environ. Model. Softw 105, 230–243. https://doi.org/10.1016/j.envsoft.2018.03.024.

Montrasio, L., Valentino, R., 2008. A model for triggering mechanisms of shallow landslides. Nat. Hazard Earth Sys. 8, 1149–1159. https://doi.org/10.5194/nhess-8-1149-2008.

Montrasio, L., Valentino, R., 2016. Modelling rainfall-induced shallow landslides at different scales using SLIP - Part II. Procedia Engineer 158, 482–486. https://doi.org/10.1016/j.proeng.2016.08.476.

Montrasio, L., Valentino, R., 2016. Modelling rainfall-induced shallow landslides at different scales using SLIP - Part I. Procedia Engineer 158, 476–481. https://doi.org/10.1016/j.proeng.2016.08.475.

Papathoma-Kohle, M., Zischg, A., Fuchs, S., Glade, T., Keiler, M., 2015. Loss estimation for landslides in mountain areas - an integrated toolbox for vulnerability assessment

and damage documentation. Environ. Model. Softw 63, 156–169. https://doi.org/10.1016/j.envsoft.2014.10.003.
Peruccacci, S., Brunetti, M.T., Gariano, S.L., Melillo, M., Rossi, M., Guzzetti, F., 2017. Rainfall thresholds for possible landslide occurrence in Italy. Geomorphology 290, 39–57. https://doi.org/10.1016/j.geomorph.2017.03.031.
Pradhan, B., Youssef, A.M., 2010. Manifestation of remote sensing data and GIS on landslide hazard analysis using spatial-based statistical models. Arab J Geosci 3, 319–326. https://doi.org/10.1007/s12517-009-0089-2.
Rodell, M., Houser, P., Jambor, U., Gottschalck, J., Mitchell, K., Meng, C.-J., Arsenault, K., Cosgrove, B., Radakovich, J., Bosilovich, M., 2004. The global land data assimilation system. Bull. Am. Meteorol. Soc. 85, 381–394.
Romanova, E., 1971. Approach of Measurement and Mapping of Soil Moisture Using Morphometric Data, Climate of Soil. Hydrometeoizdat, Leningrad (in Russian).
Sarki, A., Mirjat, M.S., Mahessar, A.A., Kori, S.M., Qureshi, A.L., 2014. Determination of saturated hydraulic conductivity of different soil texture materials. Journal of Agriculture and Veterinary Science 7, 56–62.
Shen, X., Hong, Y., 2014. CREST–The Coupled Routing and Excess STorage User Manual Version 2.1, User Manual, Hydrometeorology and Remote Sensing Laboratory, vol 25. National Weather Center, Norman, OK, USA, 25.
Sun, W.C., Wang, Y.Y., Wang, G.Q., Cui, X.Q., Yu, J.S., Zuo, D.P., Xu, Z.X., 2017. Physically based distributed hydrological model calibration based on a short period of streamflow data: case studies in four Chinese basins. Hydrol. Earth Syst. Sci. 21, 251–265. https://doi.org/10.5194/hess-21-251-2017.
Sveditchnyi, A.A., Plotnitskiy, S.V., Stepovaya, O.Y., 2003. Spatial distribution of soil moisture content within catchments and its modelling on the basis of topographic data. J. Hydrol. 277, 50–60. https://doi.org/10.1016/S0022-1694(03)00083-0.
Talebi, A., Uijlenhoet, R., Troch, P.A., 2007. Soil moisture storage and hillslope stability. Nat. Hazard Earth Sys. 7, 523–534. https://doi.org/10.5194/nhess-7-523-2007.
Tian, Y., Xiao, C.C., Liu, Y., Wu, L., 2008. Effects of raster resolution on landslide susceptibility mapping: a case study of Shenzhen. Sci. China, Ser. A 51, 188–198. https://doi.org/10.1007/s11431-008-6009-y.
Van Asch, T.W., Van Beek, L., Bogaard, T., 2007. Problems in predicting the mobility of slow-moving landslides. Eng. Geol. 91, 46–55.
van Beek, L.P.H., Wada, Y., Bierkens, M.F.P., 2011. Global monthly water stress: 1. Water balance and water availability. Water Resour. Res. 47 https://doi.org/10.1029/2010wr009791. Artn W07517.
Vogel, R.M., Fennessey, N.M., 1994. Flow-duration curves. I: new interpretation and confidence intervals. J. Water Resour. Plan. Manag. 120, 485–504.
Wada, Y., van Beek, L.P.H., Viviroli, D., Durr, H.H., Weingartner, R., Bierkens, M.F.P., 2011. Global monthly water stress: 2. Water demand and severity of water stress. Water Resour. Res. 47 https://doi.org/10.1029/2010wr009792. Artn W07518.
Wang, J.H., Yang, H., Li, L., Gourley, J.J., Sadiq, I.K., Yilmaz, K.K., Adler, R.F., Policelli, F.S., Habib, S., Irwn, D., Limaye, A.S., Korme, T., Okello, L., 2011. The coupled routing and excess storage (CREST) distributed hydrological model. Hydrol. Sci. J. 56, 84–98. https://doi.org/10.1080/02626667.2010.543087.
Wieder, W., Boehnert, J., Bonan, G., Langseth, M., 2014. Regridded Harmonized World Soil Database V1. 2. ORNL DAAC.
Wilkinson, P.L., Anderson, M.G., Lloyd, D.M., Renaud, J.P., 2002. Landslide hazard and bioengineering: towards providing improved decision support through integrated numerical model development. Environ. Model. Softw 17, 333–344. https://doi.org/10.1016/S1364-8152(01)00078-0. Pii S1364-8152(01)00078-0.
Wood, E.F., Roundy, J.K., Troy, T.J., van Beek, L.P.H., Bierkens, M.F.P., Blyth, E., de Roo, A., Doll, P., Ek, M., Famiglietti, J., Gochis, D., van de Giesen, N., Houser, P., Jaffe, P.R., Kollet, S., Lehner, B., Lettenmaier, D.P., Peters-Lidard, C., Sivapalan, M., Sheffield, J., Wade, A., Whitehead, P., 2011. Hyperresolution global land surface modeling: meeting a grand challenge for monitoring Earth's terrestrial water. Water Resour. Res. 47 https://doi.org/10.1029/2010wr010090. Artn W05301.
Xue, X.W., Hong, Y., Limaye, A.S., Gourley, J.J., Huffman, G.J., Khan, S.I., Dorji, C., Chen, S., 2013. Statistical and hydrological evaluation of TRMM-based Multi-satellite Precipitation Analysis over the Wangchu Basin of Bhutan: are the latest satellite precipitation products 3B42V7 ready for use in ungauged basins? J. Hydrol. 499, 91–99. https://doi.org/10.1016/j.jhydrol.2013.06.042.
Yao, C., Ye, J., He, Z., Bastola, S., Zhang, K., Li, Z., 2019. Evaluation of flood prediction capability of the distributed Grid-Xinanjiang model driven by WRF precipitation. Journal of Flood Risk Management, e12544.
Yao, C., Li, Z.J., Yu, Z.B., Zhang, K., 2012. A priori parameter estimates for a distributed, grid-based Xinanjiang model using geographically based information. J. Hydrol. 468, 47–62. https://doi.org/10.1016/j.jhydrol.2012.08.025.
Zhang, K., Xue, X.W., Hong, Y., Gourley, J.J., Lu, N., Wan, Z.M., Hong, Z., Wooten, R., 2016. iCRESTRIGRS: a coupled modeling system for cascading flood-landslide disaster forecasting. Hydrol. Earth Syst. Sci. 20, 5035–5048. https://doi.org/10.5194/hess-20-5035-2016.
Zhang, J., van Westen, C.J., Tanyas, H., Mavrouli, O., Ge, Y., Bajrachary, S., Gurung, D. R., Dhital, M.R., Khanal, N.R., 2018. How size and trigger matter: analyzing rainfall- and earthquake-triggered landslide inventories and their causal relation in the Koshi River basin, Central Himalaya. Nat. Hazards Earth Syst. Sci. Discuss. 1–23. https://doi.org/10.5194/nhess-2018-109, 2018a.
Zhang, K., Chao, L., Wang, Q., Huang, Y., Liu, R., Hong, Y., Tu, Y., Qu, W., Ye, J., 2019. Using multi-satellite microwave remote sensing observations for retrieval of daily surface soil moisture across China. Water Science and Engineering 12 (2), 85–97. https://doi.org/10.1016/j.wse.2019.06.001.
Zhang, Y.G., Schaap, M.G., Zha, Y.Y., 2018. A high-resolution global map of soil hydraulic properties produced by a hierarchical parameterization of a physically based water retention model. Water Resour. Res. 54, 9774–9790. https://doi.org/10.1029/2018wr023539.
Zhang, K., Wang, S., Bao, H.J., Zhao, X.M., 2019. Characteristics and influencing factors of rainfall-induced landslide and debris flow hazards in Shaanxi Province, China. Nat. Hazard Earth Sys. 19, 93–105. https://doi.org/10.5194/nhess-19-93-2019.
Zhao, R.J., 1992. The Xinanjiang model applied in China. J. Hydrol. 135, 371–381.